Author Manuscript

Author Manuscript

Author Manuscript

Author Manuscript

HHS Public Access

Author manuscript

*Microb Ecol*. Author manuscript; available in PMC 2017 January 01.

Published in final edited form as:

*Microb Ecol*. 2016 January ; 71(1): 243–255. doi:10.1007/s00248-015-0711-7.

# Phenotypic and physiological characterization of the epibiotic interaction between TM7x and its basibiont *Actinomyces*

**Batbileg Bor**[1], **Nicole Poweleit**[2], **Justin S. Bois**[3], **Lujia Cen**[1], **Joseph K. Bedree**[1], **Z. Hong Zhou**[2,4], **Robert P. Gunsalus**[2], **Renate Lux**[1], **Jeffrey S. McLean**[5], **Xuesong He**[1,*], and **Wenyuan Shi**[1,*]

[1]Section of Oral Biology, School of Dentistry, University of California, Los Angeles, CA 90095

[2]Department of Microbiology, Immunology, and Molecular Genetics, University of California, Los Angeles, CA 90095

[3]Division of Biology and Biological Engineering, California Institute of Technology, MC 114-96, Pasadena, CA 91125

[4]California Nanosystems Institute, University of California, Los Angeles, California 90095

[5]Department of Periodontics, University of Washington, Seattle, WA 98195

## Abstract

Despite many examples of obligate epibiotic symbiosis (one organism living on the surface of another) in nature, such an interaction has rarely been observed between two bacteria. Here, we further characterize a newly reported interaction between a human oral obligate parasitic bacterium TM7x (cultivated member of Candidatus Saccharimonas formerly Candidate Phylum TM7), and its basibiont *Actinomyces odontolyticus* species (XH001), providing a model system to study epiparasitic symbiosis in the domain Bacteria. Detailed microscopic studies indicate that both partners display extensive morphological changes during symbiotic growth. XH001 cells manifested as short rods in monoculture, but displayed elongated and hyphal morphology when physically associated with TM7x. Interestingly, these dramatic morphological changes in XH001 were also induced in oxygen-depleted conditions, even in the absence of TM7x. Targeted qRT-PCR analyses revealed that both the physical association with TM7x as well as oxygen depletion triggered up-regulation of key stress response genes in XH001, and in combination, these conditions act in an additive manner. TM7x and XH001 co-exist with relatively uniform cell morphologies under nutrient-replete conditions. However, upon nutrient depletion, TM7x-associated XH001 displayed a variety of cell morphologies, including swollen cell body, clubbed ends and even cell lysis, and a large portion of TM7x cells transformed from ultrasmall cocci into elongated cells. Our study demonstrates a highly dynamic interaction between epibiont TM7x and its basibiont XH001 in response to physical association or environmental cues such as oxygen level and nutritional status, as reflected by their morphological and physiological changes during symbiotic growth.

[*]Correspondence should be addressed to X.H. (xhe@g.ucla.edu) or W.S. (wenyuan@ucla.edu).

**Conflict of Interest**

The authors declare no competing financial interests.

Author Manuscript Author Manuscript Author Manuscript Author Manuscript

**Keywords**

Obligate; epibiont; symbiosis; bacterial interaction; TM7; Actinomyces

## Introduction

A recurring theme in ecology is that organisms of different species interact with each other in a variety of ways. However, intimate relationships, such as obligate epibiont symbiosis, where an organism lives exclusively on the surface of other organisms, are mainly observed between interacting pairs with at least one eukaryote [1]. Only a few examples of prokaryote-to-prokaryote obligate epibiotic interactions have been reported [2–4]. This is surprising considering the large diversity of prokaryotic organisms that have been detected by DNA sequence-based techniques [5–8]. The infrequent reporting of obligate epibiont interactions between prokaryotes can be largely explained by our inability to cultivate and study many of the microorganisms from the environment and the human body. Culturing these bacterial species in order to study their intra- and inter-species interactions is one of the major challenges in current microbiology. The ability to cultivate these species will allow for better understanding of their roles in microbial ecology, as well as microbial community-based pathogenesis.

There are numerous examples of epibiotic interactions between different bacterial species, such as phototrophic microbial consortia from lakes, corn-cob forming consortia from the oral cavity, and methane-oxidizing consortia from deep-sea sediments [9–11]. However, these symbiotic interactions are not obligate; bacteria involved in these consortia can also grow independently. To our knowledge, the only known obligate epibiotic relationships between bacterial species are predatory bacteria such as *Vampirococcus* and *Micavibrio*, and their respective bacterial prey, which include a variety of species [2, 4, 12, 13]. For this type of obligate epibiotic interaction, the predatory bacteria live on the surface of the prey and feed by leeching externally, which often results in killing of the prey in a short period of time.

Recently, we described a unique and intimate relationship between two bacterial species, TM7x (TM7 phylotype) and *Actinomyces odontolyticus* strain XH001 which were co-isolated from the human oral cavity [14]. TM7x is characterized as an obligate epibiont parasite (epiparasite) that lives on the surface of its host XH001 (referred to as the basibiont). Unlike predatory bacteria, TM7x shows a high degree of specificity for its basibiont. Furthermore, TM7x does not immediately induce cell death like most predatory bacteria, but rather maintains a stable parasitic relationship with XH001 under nutrient-replete conditions, suggesting a novel class of bacteria-to-bacteria interaction.

TM7x belongs to the TM7 phylum which, among other uncultivated phyla [15], has long been referred to as “microbial dark matter,” due to its cosmopolitan existence without a cultivable representative [14]. This phylum was recently renamed Saccharibacteria [16], after an additional TM7 genome was reconstructed from metagenomic reads and combined with the existing partial single cell TM7 genomes that were available [17, 18]. The cultivated oral TM7 described here is currently designated as Saccharibacteria oral taxon

Author Manuscript Author Manuscript Author Manuscript Author Manuscript

TM7x (NCBI Taxonomy ID: 1476577) and a complete genome has been deposited (ACCESSION CP007496) [14]. Our recent study revealed that TM7x has an ultrasmall cell size (200–300nm), a reduced genome, and is devoid of many biosynthetic pathways including *de novo* biosynthesis of all essential amino acids [14]. Moreover, the TM7 phylum was recently included in the proposed candidate phyla radiation (CPR), a subdivision of the domain Bacteria, due to these shared genomic characteristics with other novel genomes discovered in the bacterial domain [19]. Ultrasmall cells in groundwater have also been subsequently reported and suspected to belong to candidate phyla [20]. Although it is a typical constituent of the human microbiome, TM7 has been implicated in multiple human mucosal diseases such as vaginosis, inflammatory bowel disease, and periodontitis [16, 17, 21–34]. An increase in abundance of TM7 members (as high as 21% of the whole oral bacteria population in some cases) was detected in patients with various types of periodontitis [35–39]. However, little is known about the role of TM7 in the pathogenesis of these mucosal diseases.

Although it serves as a basibiont for TM7x, *A. odontolyticus* strain XH001 can also be cultured independently of TM7x [14]. Similar to many other oral *Actinomyces* spp, *A. odontolyticus* can be found among the healthy human oral flora. However, it is also considered an opportunistic pathogen and has been implicated in many diseases, such as childhood caries, periodontitis, human oral carcinomas [40–45], and most notably, Actinomycosis, the formation of painful abscesses in the mouth, lungs, or gastrointestinal tract [46, 47].

The identification of the unique TM7x/XH001 interaction provides a new model system to study obligate epiparasitic symbiosis in the domain Bacteria. In an effort to further characterize the intimate interaction between epibiont TM7x and its basibiont, we performed a detailed phenotypic and physiological analysis. Microscopic analysis revealed reciprocal morphological changes in the two interacting partners during their symbiotic growth under varying nutritional conditions. Furthermore, we demonstrate that the TM7x-induced morphological changes in XH001 can be partially recapitulated by depleting oxygen in the absence of TM7x. Most intriguingly, we present evidence suggest that TM7x-induced morphological changes in XH001 are a result of a cellular stress response and negatively affect XH001 cell growth.

## Materials and Methods

### Bacterial strains and growth conditions

XH001 monoculture and XH001/TM7x co-culture were isolated from the oral cavity as described in our previous study [14]. Strains were cultured in Brain Heart Infusion (BHI) at 37°C under different oxygen conditions as specified in the main text: anaerobic (0% $O_2$, 5% $CO_2$, 5% $H_2$, balanced with $N_2$), microaerophilic (2.6% $O_2$, 5% $CO_2$, balanced with $N_2$), high oxygen (19.7% $O_2$, 5% $CO_2$, balanced by $N_2$) and atmospheric conditions (~21% $O_2$, 0.04% $CO_2$, 0.9% Ar, 78% $N_2$). To acquire growth kinetics and phase contrast images, three independent cell cultures were grown under the specified oxygen condition for two passages (1 mL culture inoculated into 10 mL BHI and incubated 24 hours each) before being re-inoculated into 20 ml fresh BHI with a starting $OD_{600}$ of 0.03. Cells were grown for two

Author Manuscript Author Manuscript Author Manuscript Author Manuscript

passages to insure homogeneity. Subsequently, cell density was measured using Spectronic Genesys 5 spectrophotometer.

### Phase Contrast Imaging and Quantification

Phase contrast images were acquired during growth at each time point as indicated in the growth curve. At early time points, due to low cell density, we concentrated the cells by centrifugation and resuspended the cell pellets in a smaller volume of fresh medium. Cells were directly observed and imaged using Nikon Eclipse E400 microscope equipped with a Nikon Plan Fluor 100x/1.30 oil immersion objective.

For cell length and branch point analysis, XH001 monoculture and XH001/TM7x co-culture were grown in microaerophilic condition for 24 hours (after two passages) before samples were collected and observed under a phase contrast microscope. Due to the formation of micro-aggregates in XH001/TM7x co-culture, samples were treated with mild sonication (see supplementary methods) before images were acquired as described above. Images of XH001 were processed using tools available in SciPy version 0.10.0 [48] and scikit-image version 0.14.0 [49] to obtain the length and degree of branching of each bacterium.

For each image, we performed the following operations:

1. We eliminated large-scale artifacts such as uneven illumination by performing a strong Gaussian blur of the image and then subtracting this from the original image.
2. We used Otsu's method to threshold the image. Henceforth, as "region" is defined as a collection of connected pixels in a thresholded image.
3. We cleared regions that were either touching the border of the image or below a size of 50 pixels.
4. We skeletonized the image using the skimage.morphology.skeletonize function and labeled the non-adjacent skeletonized regions. These regions are only one pixel thick and may be branched.
5. For each region in the skeletonized image, we converted the pixels into a connectivity matrix, $A$, where $A _{ij} > 0$ if pixels $i$ and $ j$ are nearest neighbors. This connectivity matrix describes a graph.
6. We checked the graph for cycles. If there is a cycle, the graph is neglected. Thus, we only analyze trees. XH001 had 17/811 cycles and XH001/TM7x had 41/912.
7. Using the connectivity matrix, we computed the shortest path between each pair of pixels using the scipy.sparse.csgraph.shorestpath function.
8. Of all these shortest paths, we report the longest as the cell length.
9. Again using the connectivity matrix, we computed the number of leaves (vertices of degree one), $n _\ mathrm{leaves}$, of the branched structure. We used the number of leaves as a metric for the degree of branching. We assume we have only vertices of degree one or three, so the number of branch points (vertices of degree three) is $n _\ mathrm{leaves} – 2$.

Author Manuscript Author Manuscript Author Manuscript Author Manuscript

The source code is available upon request.

## Attachment of TM7x to XH001

Phase contrast images revealed that TM7x associated with XH001 at the highest abundance ratio when cultured under microaerophilic condition, thus this condition was used for establishing symbiotic growth. After 24 hours of growth at 37°C, 2 ml of the co-culture was re-inoculated into 20 mL fresh BHI medium, incubated for 24 hours, then followed by another 10-fold dilution in 200 ml fresh medium, and incubated for an additional 24 hours. Cells were collected by centrifugation at 13 000 × g for 10 minutes and the resulting cell pellet was re-suspended in 1 ml fresh BHI. Cell suspension was passed through 1cc Insulin Syringe (U-100 28g ½, Becton Dickinson 329410) for 10 minutes under sterile conditions to physically separate TM7x from XH001. The disassociated TM7x cells were collected by filtering the solution through a 0.22 μm Millex GP filter unit (SLGP033RB).

To re-attach TM7x to XH001, 1 ml XH001 monoculture at $OD_{600}$ of 0.2 was centrifuged at 13 000 × g for 5 minutes, and the cell pellet was re-suspended in 200 μl BHI medium containing the isolated TM7x collected as described above. Mixed cells were grown under microaerophilic conditions for 8 hours at 37°C to allow the establishment of symbiosis followed by addition of 800 μl of fresh BHI. Cultures were further incubated for 24 hours before 50 μl of the culture was re-inoculated into 2 ml fresh BHI. Cells were similarly passaged every 24 hours thereafter.

## Isolation of mRNA and construction of cDNA

For mRNA isolation, cells were grown in a 100 ml culture in BHI under the appropriate oxygen condition for 24 hours. Cells were collected by centrifugation at 13 000 × g for 5 min. Total RNA was isolated using High Pure RNA Isolation Kit (Ref 11828665001), and RNA Clean Concentrator Kit (ZYMO RESEARCH RNA Clean Concentrator: Cat#R1015) was used to clean up the RNA. Further purification of the RNA required the use of a modified version of Ambion TURBO DNA-FREE Kit protocol (Cat# AM 1907). Briefly, 1 μl of 10x TURBO DNase Buffer and DNase were added to the 6 μl of concentrated RNA. The samples were mixed gently and incubated at 37°C for 1 hour. Samples were then spiked with 1 μl of additional TURBO DNase and incubated at 37°C for 1 hour. To inactivate the DNase, 1 μl of DNase InactivationReagent was added and incubated for 5 minutes at room temperature. Sample was centrifuged at 10 000 × g for 1.5 minutes and the supernatant containing the RNA was transferred to a new tube. The RNA samples were tested for DNA contamination by PCR using universal 16S bacterial primers (015: 5′-ACTACGTGCCAGCAGCC-3′ and 016: 5′-GGACTACCAGGGTATCTAATC-3′). Once the RNA was free of DNA, it was reverse-transcribed into cDNA using Takara PrimeScript 1st strand cDNA Synthesis Kit (Cat# 6110A). The cDNA library was confirmed by PCR with universal bacterial primers (see above), *A. odontolyticus* specific 16S primers (966F: 5′-ACGGCGGCACTGCAGAGATGTG-3′ and 1410R: 5′-CCACAAACGCGGTTAGGC-3′) and TM7x specific 16S primers (400F: 5′-TATGAGTGAAGAATATGAC-3′ and 1110R: 5′-CAGTCCAAGTAGAAAAATAC-3′).

Author Manuscript Author Manuscript Author Manuscript Author Manuscript

### Quantitative Real-Time PCR (qRT-PCR)

qRT-PCR was performed using the iQ SYBR Green supermix (Bio-Rad Laboratories, Cat# 170-8882) on a Bio-Rad iQ5 real-time PCR detection system (Bio-Rad Laboratories, Inc., CA). The final qRT-PCR mixture (20 μl) contained 1× iQ SYBR Green supermix, 1μg cDNA, and 4.25 μM of the appropriate forward and reverse qRT-PCR primers (Table S1) designed for selected stress response genes. The reactions were incubated at an initial denaturation at 95°C for 3 min, followed by a 40-cycle amplification consisting of denaturation at 95 °C for 10 s, annealing at 60 °C for 30 s, and extension at 72 °C for 15 s. All primers pairs were checked for primer-dimer formation by using the dissociation curve analysis. The critical threshold cycle ($C_t$) was defined as the cycle in which fluorescence became detectable above the background fluorescence, and is inversely proportional to the logarithm of the initial number of template molecules. To calculate the fold change in mRNA expression, we used the equation developed by Michael W. Pfaffl [50]. To determine primer efficiency, a standard curve was plotted for each primer set with $C_t$ values obtained from amplification of known quantities of XH001 gDNA. We also crosschecked the sequences of the five stress genes in the TM7x genome to ensure that TM7x did not contain these sequences. Each assay was performed with at least two independent RNA samples in triplicates.

### Fluorescence *In Situ* Hybridization (FISH) imaging

FISH was carried out as previously described [14] with modifications. The cells were fixed using 4% formaldehyde for 3 hours and permeabilized by 2 mg/ml lysozyme in 20 mM Tris at pH 7.0 for 9 minutes at 37°C. Fixed cells were resuspended in 500 μl of hybridization buffer (20 mM Tris•Cl, pH8.0, 0.9 M NaCl, 0.01% SDS, 30% deionized formamide) and incubated at 37°C for 30 minutes. TM7x-specific (TM7-567: Cy5-5′-CCTACGCAACTCTTTACGCC-3′) and *A. odontolyticus*-specific (M33910: Cy3-5′-CAGTGTCGCCGTGCAT-3′) probes were used to stain the cells for 3 hours at 42°C. In Figures 5, 6 and S3, we assigned white color to Cy5-labeled TM7x to provide the best contrast. Cells were then washed three times with 0.1x saline-sodium citrate buffer, 15 minutes each, and mounted on the cover slip with SlowFade Gold anti-fade reagent (Invitrogen, Ref: S36937). Cells were visualized with a Leica SPE I inverted confocal microscope equipped with an ACS APO 100x/1.15 oil CS immersion objective. We repeated each experiment and FISH analysis at least 3 times and showed only representative images in the figures.

### Scanning Electron Microscope (SEM) sample preparation and imaging

Cells were grown overnight under the indicated gas conditions (main text) and washed with 1ml PBS. Isolation of TM7x was conducted as described above. Samples were pelleted by centrifugation at 13 000 × g for 5 minutes and resuspended in 1ml of fixative solution (3% glutaraldehyde buffered by 0.1M phosphate) and incubated at room temperature for 2–4 hours. Samples were pelleted by centrifugation and washed with 0.1M phosphate buffer four times. Samples were dehydrated with ethanol using a gradient until the water was replaced with 100% ethanol. Samples were transferred to plastic-coated copper quantifoil grids by incubation with the samples for 15 minutes. The grids were transferred to the chamber of a

Author Manuscript Author Manuscript Author Manuscript Author Manuscript

Tousimis Autosamdri-810 Critical Point Dryer and critical point drying was performed as per the manufacturer's instructions. Grids were imaged directly using the appropriate SEM holder or were adhered to SEM stubs via silver paste and coated with iridium using the South Bay Technology Ion Beam Sputtering/Etching System. Imaging was performed using a ZEISS Supra 40VP SEM operating at 1kV under high vacuum.

## Results

### Growth kinetics and morphology of XH001 as mono-species or as basibiont to TM7x

The oral cavity is a semi-oxygenated environment where saliva, supragingival tooth surfaces, and subgingival pockets harbor 40–114 (~5–15%), 60 (~8%) and 5–27 (~0.6–3.7%) mm Hg oxygen tension, respectively (in comparison, atmosphere has 155 mm Hg or 21% oxygen) [51, 52]. Therefore, we monitored the growth and morphology of XH001 as mono-species, as well as when forming symbiosis with TM7x, under microaerophilic conditions (2.6% $O_2$ and 5% $CO_2$). XH001 monoculture had a short lag-phase (~2 hours) and an approximately 16-hour exponential-phase with doubling time of ~2.5 hours (Figure 1A). The cell density plateaued at ~20 hours (stationary phase) and slowly decreased thereafter (death phase). The XH001/TM7x co-culture exhibited similar growth kinetics and plateaued around ~22 hours and had a doubling time of ~3 hours (Figure 1A). XH001 cells from monoculture displayed short rod morphology during growth (Figure 1B, a–d). However, multiple condensed spotty structures were observed throughout the cell body at later growth stages (Figure 1B, d) such as death-phase (~48 hours).

Interestingly, a more dynamic morphological change was observed in XH001 cells physically associated with TM7x. In early lag phase, TM7x-associated XH001 cells exhibited elongated and hyphal (branched) morphology (Figure 1B, e), whereas during exponential phase, the majority of the cells exhibited a short rod shape (Figure 1B, f). When entering stationary phase, the co-culture was again dominated by long and hyphal XH001 cells that were heavily decorated with TM7x (Figure 1B, g). In addition, as TM7x-associated XH001 increased in cell length during stationary phase, we also observed micro-aggregate formation (Figure S1A). During death phase, we frequently observed XH001 with large clubbed-ends, swollen cell shape, and cell lysis, which were not observed in XH001 monoculture (Figure 1B, h).

In order to validate the TM7x-induced morphological changes in XH001, we performed a re-attachment experiment. Individually isolated TM7x cells were collected by repeatedly passing the co-culture through a 28-gauge needle followed by filtering the mixture through 0.22-micron filter. The isolated TM7x cells were then co-incubated with a pure culture of XH001. Light microscopy showed that XH001 in pure culture initially manifests as short rod cells, but becomes long and hyphal after establishing the physical association with TM7x (Figure S1B–D). Our data suggests that the physical attachment with TM7x induces elongation and hyphal formation in XH001. Moreover, this association slightly decreases the apparent doubling time of XH001 compared to that of monoculture. Note that the cell density measurements of the growth curve account for both XH001 and TM7x and therefore, the decrease in the doubling time of XH001 we observe in co-culture is likely greater than represented in the graph. Additionally, the exact cell enumeration in the co-

Author Manuscript Author Manuscript Author Manuscript Author Manuscript

culture is difficult to obtain due to the micro-aggregation facilitated by the elongated XH001 cells.

### Quantification of XH001 elongation and branching

To further characterize the XH001 morphological changes that occur in the presence of TM7x, we evaluated the cell length and the number of branch points. We developed and utilized a python based software that segments the phase-contrast images followed by skeletonizing each bacterium to determine cell length and number of branch points (see Materials and Methods). The results revealed a striking difference between XH001 cells grown in monoculture and those forming a physical association with TM7x under microaerophilic condition for 24 hours. XH001 from monoculture had an average cell length of ~1.7 micrometer (μm), whereas TM7x-associated XH001 averaged ~3.7 μm (Figure 2A). Some of the XH001 cells in co-culture were as long as ~20 μm in length, while the longest XH001 cell length observed in monoculture was only ~8 μm. Furthermore, ~37% of the XH001 cells analyzed had one or more branch points during co-culture growth compared to only ~5% in monoculture. ~13% of the co-culture and ~1% of the monoculture XH001 cells had two or more branch points. Our quantitative data clearly indicate that TM7x induced significant elongation and branching in XH001.

### The effect of oxygen availability on the morphology of XH001 as monospecies or as basibiont to TM7x

Although the majority of *Actinomyces* spp., including oral species, are classified as facultative anaerobes with an obligate carbon dioxide requirement, they demonstrate a wide range of oxygen preferences and tolerances during *in vitro* culture [53]. To determine the optimal oxygen condition, XH001 monoculture and XH001/TM7x co-culture were incubated under conditions with varying oxygen and carbon dioxide concentrations. In high oxygen (19.7% $O_2$, 5% $CO_2$) conditions, both mono and co-culture displayed retarded growth compared to microaerophilic conditions (both yielding a doubling time of ~4 hours, Figure 3A, B). Under the same conditions, XH001 monoculture demonstrated short rod morphology akin to cells grown in microaerophilic conditions (Figure S2A), while in the co-culture, XH001 displayed similar elongated and hyphal morphology, although with a reduced number of associated TM7x (Figure 3C, a–d). This observation suggests that an increase in oxygen negatively impacts the growth of both XH001 and TM7x. Under normal atmospheric conditions, where oxygen is high (20.9%) and carbon dioxide concentrations are low (0.04%), XH001 in both mono and co-culture completely ceased growth (Figure 3A, B). Morphology of the XH001 in mono and co-culture under this condition assumed short branching-filaments, branching rods, and diphtheroid forms after 24 hours of growth (Figure S2B, C). Therefore, carbon dioxide is absolutely necessary for XH001, and therefore enables TM7x growth.

In anaerobic growth conditions (0% $O_2$ and 5% $CO_2$), mono or co-culture growth was decreased relative to microaerophilic conditions and plateaued at a much lower cell density (Figure 3A, B). Likewise, the co-culture had decreased growth when compared to monoculture (doubling time of ~5 and ~4 hours respectively, Figure 3A, B). Most interestingly, an XH001 monoculture incubated in anaerobic conditions exhibited elongated

Author Manuscript Author Manuscript Author Manuscript Author Manuscript

and hyphal morphology, including clubbed-ends, swollen cells, and cell lysis throughout all stages of growth comparable to the observed morphologies of XH001/TM7x co-culture experiencing nutrient depleted environments under microaerophilic condition (Figure 3D, a–d). However, these morphological alterations were reversible, switching from short rod XH001 cells to long and branched, then back to short rod morphology when oxygen levels switched from 2.6% to 0% and back to 2.6%, respectively (Figure S2D–F). The TM7x-associated XH001 cells incubated in anaerobic condition also had very similar morphology to XH001 monoculture (Figure 3D, e–h). These results indicate that the depletion of oxygen induces a cellular response in XH001 similar to the response observed when associated with TM7x.

## Association with TM7x and depletion of oxygen induces stress response in XH001 in an additive manner

Several lines of evidence suggest that the observed morphological changes in XH001 during its symbiotic growth with TM7x is likely due to a stress response: 1) Increase in cell length is generally correlated with a sub-lethal stress response [54]; 2) Our previous transcriptomic study and live/dead staining suggest that TM7x is parasitic to XH001, and may cause cell stress and a decrease in viability [14]; and 3) there is a correlation between cell elongation/branching and decreased growth rate. To test this, we performed targeted qRT-PCR to monitor the mRNA levels of five stress related genes that were up-regulated in the previous transcriptomic data (see Methods) [14]. qRT-PCR analysis revealed increased expression of *kefA*, which encodes part of the potassium efflux system, heat shock protein 60 [*groES*], and universal stress protein family in XH001 during symbiotic growth with TM7x under microaerophilic conditions. The expression of genes encoding Chaperone protein DnaJ and putative NADPH-quinone reductase was not changed compared to XH001 monoculture (Figure 4). Meanwhile, the XH001 monoculture under anaerobic conditions showed even higher mRNA expression levels of all genes except NADPH-quinone reductase compared to co-culture, suggesting that stress induced by oxygen depletion is more severe than that caused by establishing an epiparasitic relationship with TM7x under microaerophilic conditions. Most intriguingly, when serving as basibiont for TM7x and incubated in an anaerobic condition, XH001 displayed the most drastic increase in all stress response genes evaluated, with several genes increasing 1000-fold or higher, indicating an additive effect of these conditions. These results suggest that the XH001 morphological changes due to TM7x binding or depletion of oxygen are likely a result of a cellular stress response.

## Morphological changes in TM7x during epibiotic growth with XH001

The low resolution of the phase contrast microscope allowed us to characterize the morphology of XH001, but not TM7x. To monitor the possible morphological changes in TM7x, which are ultrasmall cocci with a diameter of 200–300 nm (measured previously by Transmission Electron Microscope (TEM)) during early symbiotic growth with XH001 [14], we employed Fluorescence *In Situ* Hybridization (FISH) staining followed by fluorescence confocal microscopy. To distinguish between XH001 and TM7x, we developed fluorescently tagged XH001- and TM7x-specific FISH probes targeting the 16S rRNA gene. Using these probes, we visualized the morphology of TM7x associated with XH001 over different growth phases under microaerophilic conditions. As expected, XH001 monoculture

Author Manuscript Author Manuscript Author Manuscript Author Manuscript

cells exhibited short rod morphology when stained with an XH001-specific probe throughout all stages of growth (Figure S3A, only 24 hr shown). We did not observe non-specific staining of XH001 monoculture with TM7x specific probes (Figure S3A). During lag, exponential, and stationary phase of the co-culture, TM7x mostly appeared as cocci with a diameter of 0.5–1 μm, although we also observed a slightly elongated form of TM7x (1–2μm) that is much smaller than XH001 (Figure 5A–C). Cocci cell diameter, however, is different from our previous measurements as well as measurements through SEM imaging (200–300 nm, see following section). The observed discrepancy is likely due to the low quality resolution of the FISH images. Consistent with our phase contrast images, TM7x associated XH001 frequently displayed elongated and hyphal morphology except during exponential phase, where short rod morphology dominated (Figure 5B). During death phase, in addition to cocci and short rods, we also observed elongated TM7x cells that were 2–5 μm in length (Figure 5D). These elongated forms of TM7x were also enriched in the XH001/TM7x co-culture grown in anaerobic conditions (Figure 3D, g, h, 5E, S3C). Our FISH imaging does not clearly indicate whether these are chains of multiple cells or a single, elongated TM7x cell. Similar to the phase contrast images, XH001 in mono and co-culture under anaerobic conditions demonstrated elongated and hyphal morphology, as well as clubbed-ends and swollen cell shape (Figure S3B, C). Moreover, FISH imaging showed non-uniform staining of XH001, possibly due to leakage of cytoplasmic content, which supports the hypothesis that XH001 is highly stressed in an anaerobic environment (Figure S3B, C).

Fluorescent images also revealed that individual TM7x cells decorating XH001 could be classified into distinct subsets based on their morphology. Specifically, TM7x morphology ranged from cocci (Figure 6A), cocci with various tail lengths (Figure 6B–D), two connected cocci (Figure 6E), or two slightly separated cocci (Figure 6F). These distinct morphologies can be observed during all growth phases and suggest that TM7x may undergo bud formation and growth.

## Morphology of XH001 and TM7x under Scanning Electron Microscopy (SEM)

To acquire more detailed knowledge of the morphological dynamics of XH001 and TM7x, SEM was used to visualize XH001 and TM7x. SEM images confirmed the short rod appearance of XH001 in monoculture as well as the more elongated and branched morphology of XH001 in co-culture that is heavily decorated with TM7x (Figure 7A, B). XH001 in mono and co-culture in a microaerophilic and nutrient rich condition displayed smooth cell surfaces without any appendages (pili and/or flagella). Similar to our FISH images, SEM revealed TM7x cells with different morphologies, such as short rods as well as elongated cells. Notably, the TM7x morphology resembled budding yeast or budding bacteria (Figure 7B inset) [55, 56], supporting our speculation that TM7x growth occurs by budding. Furthermore, when TM7x cells were isolated from co-culture using a 0.22-micron filter, SEM images revealed individual, non-XH001 attached TM7x with a coccoid morphology with a diameter of ~200 nm (Figure 7C), confirming our previous measurements with TEM sections [14]. Cells grown in anaerobic conditions exhibited aggregation under SEM, consistent with our phase contrast and FISH images (Figure 7D). Nevertheless, we were still able to visualize the elongated morphologies of XH001 and

Author Manuscript Author Manuscript Author Manuscript Author Manuscript

TM7x. Some of the XH001 cells appeared contracted with pitted surfaces (data not shown), reflecting a potential stressed state. Similar “stress-related” cell surface morphologies have been reported in other bacteria, but with less severe changes in the membrane surface [57, 58]. Overall, the SEM images validated our observation of elongated and branched XH001, and further revealed that stressed XH001 has uneven surfaces.

## Discussion

Using novel cultivation methods, a member of the Phylum Candidatus Saccharibacteria (formerly TM7) was recently isolated from the human oral cavity (designated Candidatus Saccharibacteria oral taxon TM7x) as an obligate epibiont parasite growing on the surface of its host bacterial species *A. odontolyticus* (XH001) [14]. In this study, we further reveal the dynamic interaction between the two partners, as reflected by their reciprocal morphological changes and induction of stress genes during co-culture growth. Elongation and cell branching were the most substantial morphological changes in XH001 induced by the symbiotic association of TM7x. Previous studies have indicated that *Actinomyces* spp. assumes different morphologies ranging from short curved rods to filamentous hyphal cells. Other morphologies include, but are not limited to, clubbed-ends, diphtheroid arrangements, short chains, small clusters such as spider colonies, and coccoid shape [53]. These cell morphologies are thought to be dynamic and determined by different environmental conditions such as growth media and temperature [53]. Our findings are consistent with these studies to the extent that XH001 can take different cell morphologies when experiencing different growth conditions. More importantly, we determined that the observed transformation from short rods to elongated and branched morphology in XH001 is likely a result of a cellular stress response induced by TM7x, as revealed by our targeted qRT-PCR analysis (Figure 4, 8a). To our knowledge, this is the first evidence that cell stress is linked to elongated and hyphal morphology of *Actinomyces* species. Intriguingly, these morphological changes, as well as up-regulation of stress-related gene expression, can be recapitulated in a heightened manner by incubating XH001 monoculture in anaerobic conditions (Figure 8b). This is an indication that TM7x and anaerobic environments may induce similar morphological changes in XH001 as a result of the same cellular stress response. Supporting this hypothesis, association with TM7x and cultivation under anaerobic conditions resulted in an additive effect on the up-regulation of stress response genes in XH001 (Figure 8c). However, the molecular mechanisms by which TM7x association or anaerobic environment induces the stress response have yet to be elucidated.

In many bacterial species, one of the main cellular responses to external insults or internal stress is elongation of the cell body [54]. In the current study, we reveal a novel culprit for induction of the stress response, XH001’s obligate epibiotic partner, TM7x. Since TM7x is an epibiotic parasite that exists on the surface of its basibiont, we speculate that the induction of the stress response in XH001 that results in cell elongation allows TM7x greater surface area in which to grow. Under nutrition-replete conditions, TM7x causes moderate elongation and branching in XH001 presumably by keeping its basibiont relatively healthy (Figure 8a). The balance between achieving greater surface area for growth and maintaining basibiont viability plays an important role in determining the success of the epibiotic relationship. Under nutrition-depleted conditions, however, the balance shifts, with

Author Manuscript Author Manuscript Author Manuscript Author Manuscript

TM7x causing severe cell morphology and cell lysis in XH001, similar to that of a predatory bacteria (Figure 8c). In plant symbiosis, the terms biotroph (a parasite that depends on the host's survival), necrotroph (a parasite that kills the host) and hemi-biotrophs (a parasite that displays characteristics of both) are used regularly [59]. These terms can be applied to bacterial symbiosis, as we see the relationship between TM7x and XH001 shift from biotrophic (early nutrient replete-condition) to necrotrophic (late nutrient deplete-condition), which is in contrast to predatory bacteria in which the interaction is mainly dominated by a necrotrophic relationship. It is fascinating that biotrophic and necrotrophic symbiosis not only exists in higher organisms, but also among the most basic life forms, bacteria. Future studies are needed to explore this dynamic interaction between TM7x and XH001 at the molecular and genetic level.

TM7x grows dependently on the surface of basibiont XH001 and has different morphologies, such as cocci and a filamentous cell body. More intriguingly, our data suggest that TM7x might divide by budding. The FISH and SEM images clearly reveal TM7x morphologies that may reflect different budding stages (Figure 6 and 7). Without analyzing large number of cells, however, we could not determine if the different morphologies are correlated with specific growth phases. Previous studies show that Alpha-proteobacteria *Hyphomonas*, *Pedomicrobium* and *Ancalomicrobium*, as well as *Planctomyces maris* grow by budding [56], although they are all free-living bacteria. In contrast, TM7x seems to bud while attached to XH001. Future studies are needed to understand the mechanism of budding and the physical association of TM7x with XH001. In addition, we also observed an elongated form of TM7x. This morphology was observed most frequently when the co-culture was incubated under microaerophilic conditions for long periods of time (nutrient-depleted) or incubated under anaerobic conditions (Figure 8c), suggesting that elongation of TM7x may also be a result of a stress response.

Both *A. odontolyticus* and TM7 are known members of the healthy bacterial flora of the oral cavity with increased abundance in certain disease conditions. The intimate interaction between TM7x and XH001 demonstrated in our study offers a glimpse into additional ways bacteria may interact with each other within the oral cavity and possibly in other body sites where TM7 members are detected. This unique interaction provides a great model system for understanding the intricacies of bacteria-to-bacteria hemi-biotrophic symbiosis and the impact of this interaction relative to bacterial ecologically-induced human diseases.

## Supplementary Material

Refer to Web version on PubMed Central for supplementary material.

## Acknowledgments

We thank the members of the Shi and Lux laboratories for their feedback and invaluable discussion. We also thank Melissa Agnello for providing extensive editing of the manuscript. We thank the Chemistry and Biochemistry instrumentation facility at UCLA for providing access to the confocal microscope. This work was supported in part by grants from the National Institutes of Health (1R01DE023810-01) and Oral Health-Research Postdoctoral Training Program (B.B., UCLA School of Dentistry T90 award).

Author Manuscript Author Manuscript Author Manuscript Author Manuscript

## References


1. Joseph, S. Symbiosis: Mechanisms and Model Systems. Kluwer Academic Publisher; New York, Boston, Dordrecht, London, Moscow: 2002.
2. Guerrero R, Pedros-Alio C, Esteve I, et al. Predatory prokaryotes: predation and primary consumption evolved in bacteria. Proc Natl Acad Sci. 1986; 83:2138–2142.10.1073/pnas.83.7.2138 [PubMed: 11542073]
3. Huber H, Hohn MJ, Rachel R, et al. A new phylum of Archaea represented by a nanosized hyperthermophilic symbiont. Nature. 2002; 417:63–67.10.1038/417063a [PubMed: 11986665]
4. Lambina VA, Afinogenova AV, Romaĭ Penabad S, et al. *Micavibrio admirandus* gen. et sp. nov. Mikrobiologiia. 1982; 51:114–117. [PubMed: 7070304]
5. Grice EA, Segre JA. The human microbiome: our second genome. Annu Rev Genomics Hum Genet. 2012; 13:151–170.10.1146/annurev-genom-090711-163814 [PubMed: 22703178]
6. Human Microbiome Project Consortium. Structure, function and diversity of the healthy human microbiome. Nature. 2012; 486:207–214.10.1038/nature11234 [PubMed: 22699609]
7. Roesch LFW, Fulthorpe RR, Riva A, et al. Pyrosequencing enumerates and contrasts soil microbial diversity. ISME J. 2007; 1:283–290.10.1038/ismej.2007.53 [PubMed: 18043639]
8. Schauer R, Bienhold C, Ramette A, Harder J. Bacterial diversity and biogeography in deep-sea surface sediments of the South Atlantic Ocean. ISME J. 2010; 4:159–170.10.1038/ismej.2009.106 [PubMed: 19829317]
9. Bryant MP, Wolin EA, Wolin MJ, Wolfe RS. *Methanobacillus omelianskii*, a symbiotic association of two species of bacteria. Arch Für Mikrobiol. 1967; 59:20–31.
10. Lancy P, Dirienzo JM, Appelbaum B, et al. Corncob formation between *Fusobacterium nucleatum* and *Streptococcus sanguis*. Infect Immun. 1983; 40:303–309. [PubMed: 6131871]
11. Overmann J. The phototrophic consortium "*Chlorochromatium aggregatum*" - a model for bacterial heterologous multicellularity. Adv Exp Med Biol. 2010; 675:15–29.10.1007/978-1-4419-1528-3_2 [PubMed: 20532733]
12. Davidov Y, Huchon D, Koval SF, Jurkevitch E. A new *Alpha-proteobacterial* clade of *Bdellovibrio*-like predators: implications for the mitochondrial endosymbiotic theory. Environ Microbiol. 2006; 8:2179–2188.10.1111/j.1462-2920.2006.01101.x [PubMed: 17107559]
13. Dashiff A, Junka RA, Libera M, Kadouri DE. Predation of human pathogens by the predatory bacteria *Micavibrio aeruginosavorus* and *Bdellovibrio bacteriovorus*. J Appl Microbiol. 2011; 110:431–444.10.1111/j.1365-2672.2010.04900.x [PubMed: 21114596]
14. He X, McLean JS, Edlund A, et al. Cultivation of a human-associated TM7 phylotype reveals a reduced genome and epibiotic parasitic lifestyle. Proc Natl Acad Sci U S A. 2015; 112:244–249.10.1073/pnas.1419038112 [PubMed: 25535390]
15. Lasken RS, McLean JS. Recent advances in genomic DNA sequencing of microbial species from single cells. Nat Rev Genet. 2014; 15:577–584.10.1038/nrg3785 [PubMed: 25091868]
16. Albertsen M, Hugenholtz P, Skarshewski A, et al. Genome sequences of rare, uncultured bacteria obtained by differential coverage binning of multiple metagenomes. Nat Biotechnol. 2013; 31:533–538.10.1038/nbt.2579 [PubMed: 23707974]
17. Marcy Y, Ouverney C, Bik EM, et al. Dissecting biological "dark matter" with single-cell genetic analysis of rare and uncultivated TM7 microbes from the human mouth. Proc Natl Acad Sci. 2007; 104:11889–11894.10.1073/pnas.0704662104 [PubMed: 17620602]
18. Podar M, Abulencia CB, Walcher M, et al. Targeted Access to the Genomes of Low-Abundance Organisms in Complex Microbial Communities. Appl Environ Microbiol. 2007; 73:3205–3214.10.1128/AEM.02985-06 [PubMed: 17369337]
19. Brown CT, Hug LA, Thomas BC, et al. Unusual biology across a group comprising more than 15% of domain Bacteria. Nature. 201510.1038/nature14486
20. Luef B, Frischkorn KR, Wrighton KC, et al. Diverse uncultivated ultra-small bacterial cells in groundwater. Nat Commun. 2015; 6:6372.10.1038/ncomms7372 [PubMed: 25721682]
21. Bik EM, Eckburg PB, Gill SR, et al. Molecular analysis of the bacterial microbiota in the human stomach. Proc Natl Acad Sci. 2006; 103:732–737.10.1073/pnas.0506655103 [PubMed: 16407106]

Author Manuscript Author Manuscript Author Manuscript Author Manuscript


22. Dewhirst FE, Chen T, Izard J, et al. The human oral microbiome. J Bacteriol. 2010; 192:5002–5017.10.1128/JB.00542-10 [PubMed: 20656903]
23. Dinis JM, Barton DE, Ghadiri J, et al. In search of an uncultured human-associated TM7 bacterium in the environment. PloS One. 2011; 6:e21280.10.1371/journal.pone.0021280 [PubMed: 21701585]
24. Eckburg PB, Bik EM, Bernstein CN, et al. Diversity of the human intestinal microbial flora. Science. 2005; 308:1635–1638.10.1126/science.1110591 [PubMed: 15831718]
25. Ferrari BC, Binnerup SJ, Gillings M. Microcolony cultivation on a soil substrate membrane system selects for previously uncultured soil bacteria. Appl Environ Microbiol. 2005; 71:8714–8720.10.1128/AEM.71.12.8714-8720.2005 [PubMed: 16332866]
26. Fredricks DN, Fiedler TL, Marrazzo JM. Molecular identification of bacteria associated with bacterial vaginosis. N Engl J Med. 2005; 353:1899–1911.10.1056/NEJMoa043802 [PubMed: 16267321]
27. Gao Z, Tseng C, Pei Z, Blaser MJ. Molecular analysis of human forearm superficial skin bacterial biota. Proc Natl Acad Sci. 2007; 104:2927–2932.10.1073/pnas.0607077104 [PubMed: 17293459]
28. Hanada A, Kurogi T, Giang NM, et al. Bacteria of the candidate phylum TM7 are prevalent in acidophilic nitrifying sequencing-batch reactors. Microbes Environ JSME. 2014; 29:353–362.10.1264/jsme2.ME14052
29. Hugenholtz P, Tyson GW, Webb RI, et al. Investigation of candidate division TM7, a recently recognized major lineage of the domain Bacteria with no known pure-culture representatives. Appl Environ Microbiol. 2001; 67:411–419.10.1128/AEM.67.1.411-419.2001 [PubMed: 11133473]
30. Kianoush N, Adler CJ, Nguyen K-AT, et al. Bacterial profile of dentine caries and the impact of pH on bacterial population diversity. PloS One. 2014; 9:e92940.10.1371/journal.pone.0092940 [PubMed: 24675997]
31. Kuehbacher T, Rehman A, Lepage P, et al. Intestinal TM7 bacterial phylogenies in active inflammatory bowel disease. J Med Microbiol. 2008; 57:1569–1576.10.1099/jmm.0.47719-0 [PubMed: 19018031]
32. Paster BJ, Boches SK, Galvin JL, et al. Bacterial diversity in human subgingival plaque. J Bacteriol. 2001; 183:3770–3783.10.1128/JB.183.12.3770-3783.2001 [PubMed: 11371542]
33. Rheims H, Spröer C, Rainey FA, Stackebrandt E. Molecular biological evidence for the occurrence of uncultured members of the *Actinomycete* line of descent in different environments and geographical locations. Microbiol Read Engl. 1996; 142(Pt 10):2863–2870.10.1099/13500872-142-10-2863
34. Soro V, Dutton LC, Sprague SV, et al. Axenic culture of a *Candidate* division TM7 bacterium from the human oral cavity and biofilm interactions with other oral bacteria. Appl Environ Microbiol. 2014; 80:6480–6489.10.1128/AEM.01827-14 [PubMed: 25107981]
35. Brinig MM, Lepp PW, Ouverney CC, et al. Prevalence of bacteria of division TM7 in human subgingival plaque and their association with disease. Appl Environ Microbiol. 2003; 69:1687–1694.10.1128/AEM.69.3.1687-1694.2003 [PubMed: 12620860]
36. Kumar PS, Griffen AL, Barton JA, et al. New bacterial species associated with chronic periodontitis. J Dent Res. 2003; 82:338–344. [PubMed: 12709498]
37. Liu B, Faller LL, Klitgord N, et al. Deep sequencing of the oral microbiome reveals signatures of periodontal disease. PLoS ONE. 2012; 7:e37919.10.1371/journal.pone.0037919 [PubMed: 22675498]
38. Paster BJ, Russell MK, Alpagot T, et al. Bacterial diversity in necrotizing ulcerative periodontitis in HIV-positive subjects. Ann Periodontol Am Acad Periodontol. 2002; 7:8–16.10.1902/annals.2002.7.1.8
39. Rylev M, Bek-Thomsen M, Reinholdt J, et al. Microbiological and immunological characteristics of young Moroccan patients with aggressive periodontitis with and without detectable *Aggregatibacter actinomycetemcomitans* JP2 infection. Mol Oral Microbiol. 2011; 26:35–51.10.1111/j.2041-1014.2010.00593.x [PubMed: 21214871]
40. Becker MR, Paster BJ, Leys EJ, et al. Molecular analysis of bacterial species associated with childhood caries. J Clin Microbiol. 2002; 40:1001–1009. [PubMed: 11880430]

Author Manuscript Author Manuscript Author Manuscript Author Manuscript


41. Colombo AV, Silva CM, Haffajee A, Colombo APV. Identification of oral bacteria associated with crevicular epithelial cells from chronic periodontitis lesions. J Med Microbiol. 2006; 55:609–615.10.1099/jmm.0.46417-0 [PubMed: 16585650]
42. Kanasi E, Dewhirst FE, Chalmers NI, et al. Clonal analysis of the microbiota of severe early childhood caries. Caries Res. 2010; 44:485–497.10.1159/000320158 [PubMed: 20861633]
43. Ling Z, Kong J, Jia P, et al. Analysis of oral microbiota in children with dental caries by PCR-DGGE and barcoded pyrosequencing. Microb Ecol. 2010; 60:677–690.10.1007/s00248-010-9712-8 [PubMed: 20614117]
44. Nagy KN, Sonkodi I, Szöke I, et al. The microflora associated with human oral carcinomas. Oral Oncol. 1998; 34:304–308. [PubMed: 9813727]
45. Sato T, Watanabe K, Kumada H, et al. Peptidoglycan of *Actinomyces naeslundii* induces inflammatory cytokine production and stimulates osteoclastogenesis in alveolar bone resorption. Arch Oral Biol. 2012; 57:1522–1528.10.1016/j.archoralbio.2012.07.012 [PubMed: 22939375]
46. Aas JA, Paster BJ, Stokes LN, et al. Defining the normal bacterial flora of the oral cavity. J Clin Microbiol. 2005; 43:5721–5732.10.1128/JCM.43.11.5721-5732.2005 [PubMed: 16272510]
47. Paul, D.; Reddy, D.; Mukherjee, D., et al. Actinomyces. In: Liu, D., editor. Mol Detect Hum Bact Pathog. CRC Press; 2011. p. 23-30.
48. Jones, E.; Oliphant, E.; Peterson, P., et al. SciPy: Open source scientific tools for python. 2001. http://www.scipy.org/
49. Walt S, Schonberger JL, Nunez-Iglesias J, et al. Scikit-image: Image processing in Pythong. PeerJ. 2014; 2:e453. http://dx.doi.org/10.7717/peerj.453. [PubMed: 25024921]
50. Pfaffl MW. A new mathematical model for relative quantification in real-time RT-PCR. Nucleic Acids Res. 2001; 29:e45. [PubMed: 11328886]
51. Hill, MJ.; Marsh, PD. Hum Microb Ecol. CRC Press. Inc; 1990. Factors controlling the microflora of the huealthy mouth; p. 34-37.
52. Loesche WJ, Gusberti F, Mettraux G, et al. Relationship between oxygen tension and subgingival bacterial flora in untreated human periodontal pockets. Infect Immun. 1983; 42:659–667. [PubMed: 6642647]
53. Schaal, KP.; Yassin, AA. Bergeys Man Syst Bacteriol. Springer; 2012. Genus I. *Actinomyces*; p. 42-109.
54. Jones TH, Vail KM, McMullen LM. Filament formation by foodborne bacteria under sublethal stress. Int J Food Microbiol. 2013; 165:97–110.10.1016/j.ijfoodmicro.2013.05.001 [PubMed: 23727653]
55. Herskowitz, Ira. Life cycle of the budding yeast *Saccharomyces cerevisiae*. Microbiol Rev. 1988; 52:536–553. [PubMed: 3070323]
56. Hirsch, Peter. Budding bacteria. Annu Rev Microbiol. 1974; 28:391–440. [PubMed: 4611332]
57. Greif D, Wesner D, Regtmeier J, Anselmetti D. High resolution imaging of surface patterns of single bacterial cells. Ultramicroscopy. 2010; 110:1290–1296.10.1016/j.ultramic.2010.06.004 [PubMed: 20558001]
58. Patil S, Valdramidis VP, Karatzas KaG, et al. Assessing the microbial oxidative stress mechanism of ozone treatment through the responses of *Escherichia coli* mutants. J Appl Microbiol. 2011; 111:136–144.10.1111/j.1365-2672.2011.05021.x [PubMed: 21457413]
59. Glazebrook J. Contrasting mechanisms of defense against biotrophic and necrotrophic pathogens. Annu Rev Phytopathol. 2005; 43:205–227.10.1146/annurev.phyto.43.040204.135923 [PubMed: 16078883]

Author Manuscript Author Manuscript Author Manuscript Author Manuscript

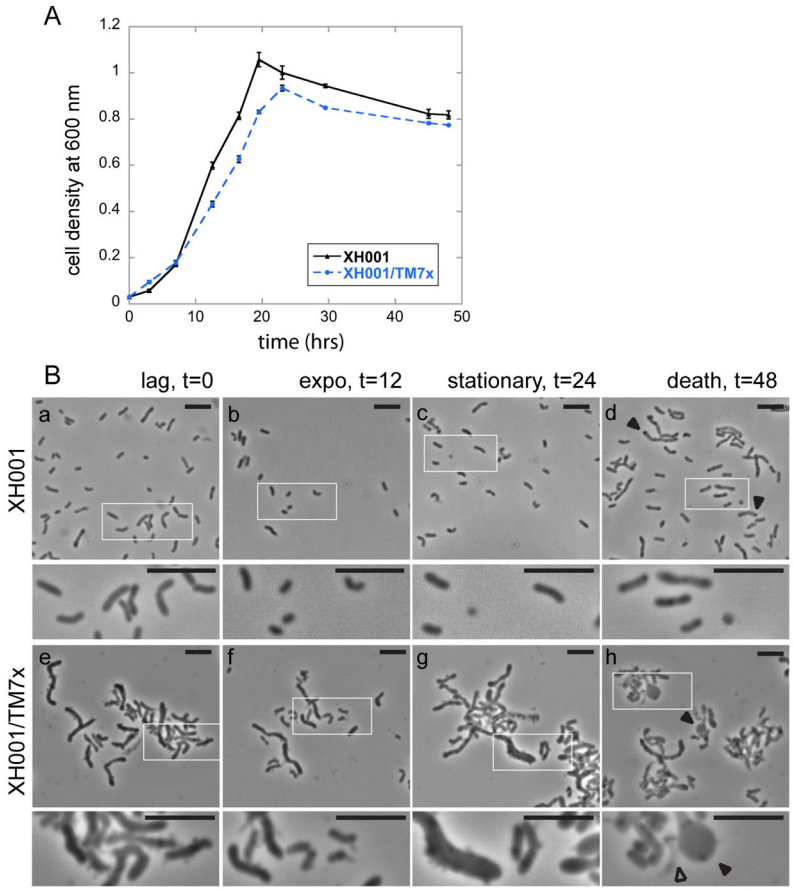


**Figure 1.**

Growth and morphology of XH001 monoculture and XH001/TM7x co-culture. (A) Mono (triangle, black solid line) and co-culture (circle, blue broken line) cell densities were determined by measuring the optical density at 600 nm ($OD_{600}$). Each point represents the average of three independent cultures (error bars, SD). The time points were connected by straight line to guide the eye. (B, a–d) XH001 monoculture grown in microaerophilic conditions has short rod morphology from early to late growth phases. The lower images are a higher magnification of the boxed region in the upper image. During death phase (B, d), many of the cells had condensed dot structures within the cell body (arrow heads). (B, e–h) TM7x-associated XH001 have elongated and hyphal morphology from early to late growth phases. During exponential phase (B, f), many of the XH001 cells are short rods similar to XH001 alone. At death phase (B, h), many of the XH001 cells display large clubbed-ends (arrow heads), swollen cells, and cell lyses (open arrow head). During all growth phases, XH001 was heavily decorated with TM7x. All scale bars indicate 5 μm.

Author Manuscript Author Manuscript Author Manuscript Author Manuscript

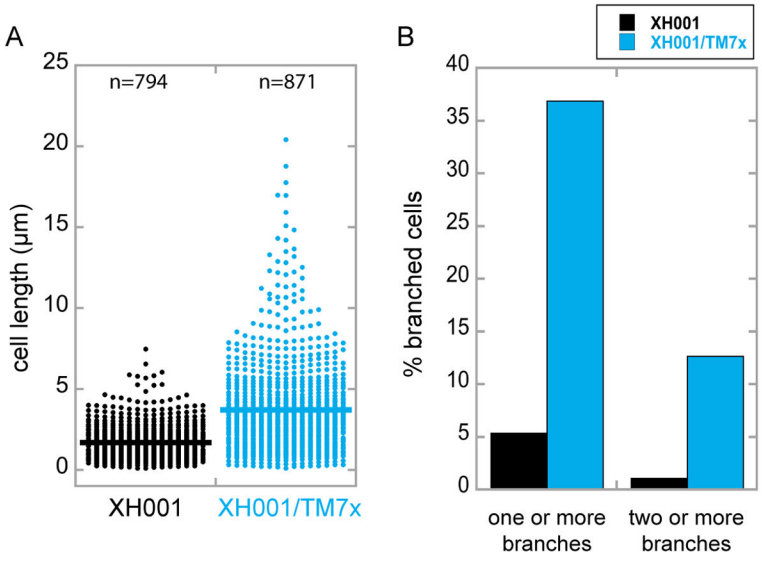


**Figure 2.**

Quantification of cell length and branch points in TM7x associated XH001. Mild sonication-dispersed co-culture cells were quantified by python-based image analysis software (see Materials and Methods) that automatically quantifies the longest length of the XH001 cells, and number of branch points. (A) n is the total number of cells measured from multiple microscope slides prepared from three independent mono or co-cultures incubated under microaerophilic conditions. Error bars are not shown as we combined the data to show the cell length distribution. Student's t-test was used to determine significance ($p<0.001$) (B) Each bar shows the percent of cells in A (from n cells) that had one or more, or two or more branch points. TM7x-associated XH001 is ~7 times more likely to have one or more branch points or ~13 times more likely to have two or more branch points compare to XH001 alone.

Author Manuscript Author Manuscript Author Manuscript Author Manuscript

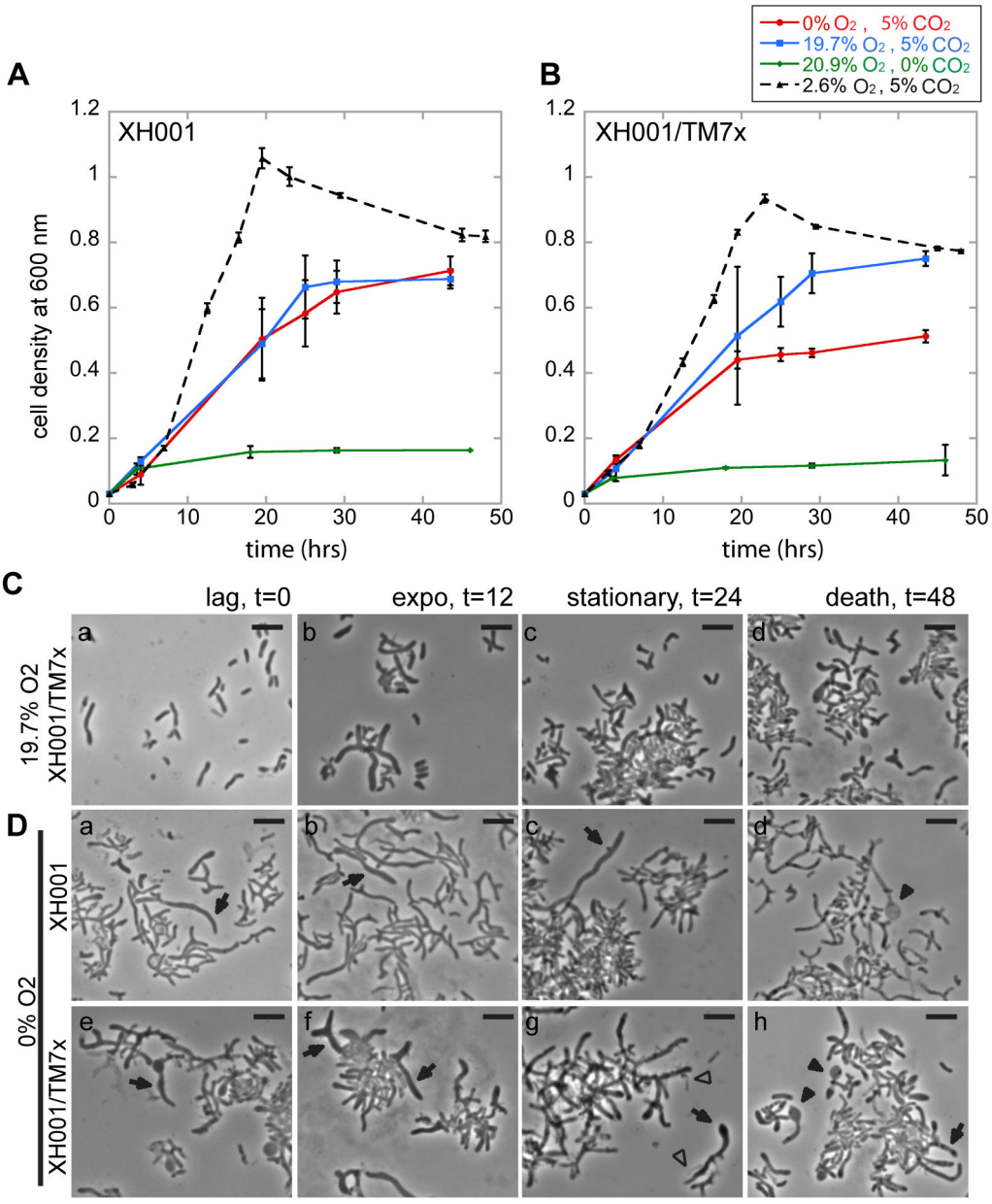


**Figure 3.**

Oxygen depletion-induced morphological changes in XH001 mono and co-cultures. (A–B) Cell density measurements of XH001 mono (A) or co-culture (B) under microaerophilic (2.6% $O_2$, 5% $CO_2$, triangles, black broken line), high oxygen (19.7% $O_2$, 5% $CO_2$, squires, blue solid line), atmospheric (20.9% $O_2$, 0.04% $CO_2$, diamonds, green solid line) or anaerobic (0% $O_2$, 5% $CO_2$, circles, red solid lines) conditions. The dashed lines are the same data points from Figure 1. Each point represents the average of three independent cultures (error bars, SD). (C, D) Phase contrast images of cells grown under indicated conditions (see also Figure S2). (C, a–d) Co-culture grown under high oxygen condition for indicated amount of time. XH001 alone (D, ad) or with TM7x (D, e–h) grown under anaerobic condition for indicated amount of time. In these images, we can clearly see

clubbed-ended (filled arrow heads) and swollen (arrows) XH001 cells as well as elongated TM7x cells (open arrow heads). All scale bars indicate 5 μm.

Author Manuscript Author Manuscript Author Manuscript Author Manuscript

Author Manuscript Author Manuscript Author Manuscript Author Manuscript

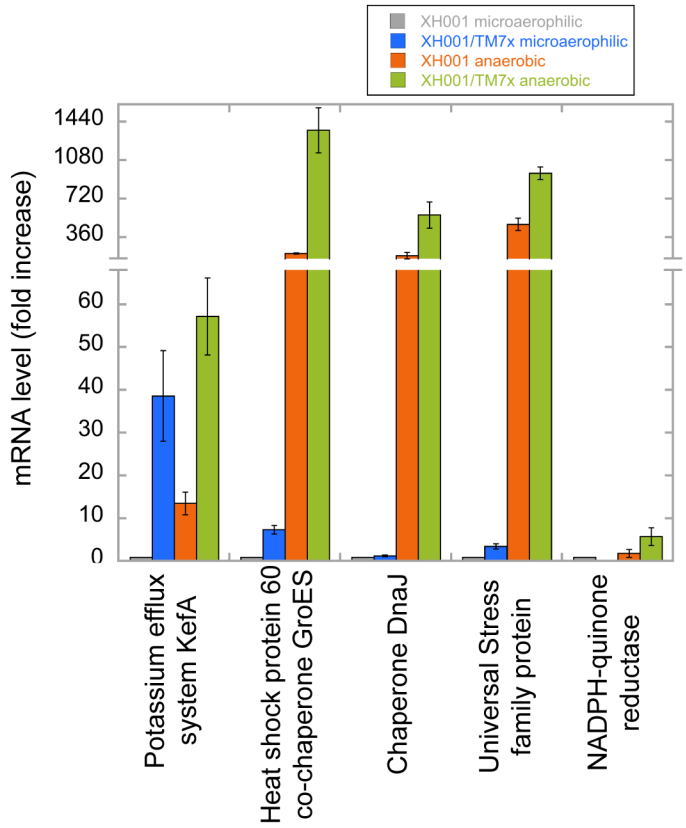


**Figure 4.**

Stress response of XH001 under TM7x-associated and/or anaerobic conditions. We tested mRNA levels of 5 stress genes using qRT-PCR in XH001 grown with TM7x under microaerophilic (blue) or anaerobic conditions (green), or XH001 alone grown under anaerobic conditions (orange), and compared that to XH001 monoculture grown under microaerophilic conditions (gray). Each bar represents the average of three independent experiments (error bars, SD).

Author Manuscript Author Manuscript Author Manuscript Author Manuscript

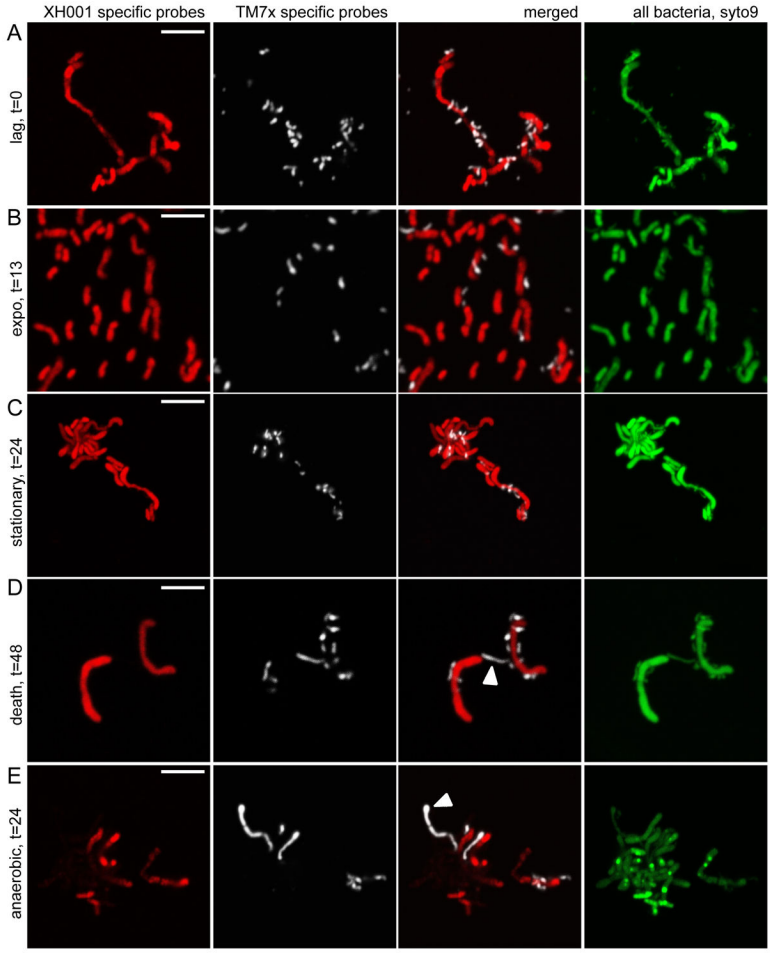


**Figure 5.**

Morphology of TM7x during growth. Co-culture grown under microaerophilic conditions was FISH stained using TM7x-specific (white, TM7567) and XH001-specific (red, M33910) DNA-probes that target the 16S rRNA gene (see Materials and Methods). Green is a universal DNA dye, syto9, which stains both XH001 and TM7x DNA and RNA. XH001 monoculture staining is shown in Figure S3. At time points 0 (A), 24 (C) and 48 (D) hours, XH001 had long and hyphal morphology. At 13 hours (B), many of the XH001 cells were short rods. TM7x also assumed different morphologies. At time points 0–24 (A–C) hours, TM7x appeared as small cocci or short rods. At 48 hours (D), the elongated form of TM7x was observed more frequently (white arrow head). (E) Interestingly, TM7x also assumed an elongated morphology when the co-culture was incubated under anaerobic conditions (white arrowhead). Long TM7x can be observed throughout all time points of the growth but only t = 24 hours is shown in E. All scale bars indicate 5 μm.

Author Manuscript Author Manuscript Author Manuscript Author Manuscript

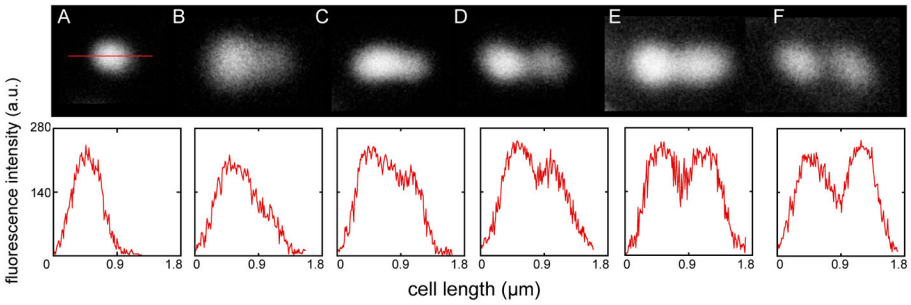


**Figure 6.**

Bud-like morphology of TM7x. (A–F) Magnified images of TM7x from the co-culture stained with a TM7x-specific FISH probe. Representative images were selected from FISH staining of co-culture grown under microaerophilic conditions. These images are not a time series, but rather a collection of different cells from the FISH imaging. XH001 staining is not shown. Different stages of bud growth can be seen throughout all time points of the co-culture growth. These images were further analyzed by graphing the length (x-axes) versus fluorescent intensity of Cy-5-TM7567 (y-axes) along the red line drawn across the budding cells (see red line in A). (A) Representative image of cocci TM7x is shown. (B) Very beginning of bud formation is shown by one large coccus with a small tail-like formation. (C) Further bud development is evidenced by a clearer tail-like formation. (D) Two connected cells are represented. One cell is smaller than the other, possibly formed from the tail-like structure. (E) Two cells that have clear separation but still connected by weak fluorescent signal. (F) Finally, two cells that are separated and have clear boundaries. The scale bar in the images are not displayed since the graph is accurately showing the cell length.

Author Manuscript Author Manuscript Author Manuscript Author Manuscript

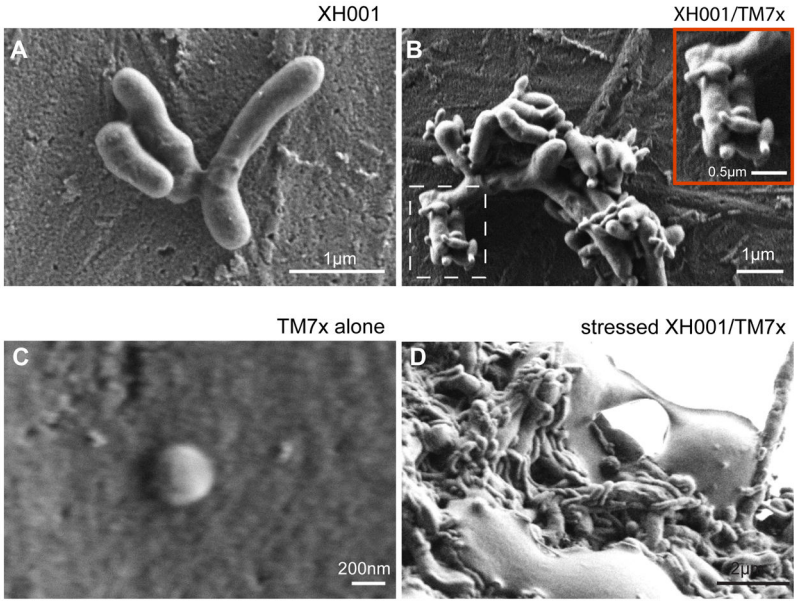


**Figure 7.**

Morphology of XH001 and TM7x under SEM. (A) XH001 monoculture grown under microaerophilic conditions shows short rod morphology with smooth surfaces. (B) Co-culture grown under microaerophilic conditions reveals elongated and branched XH001 cells decorated with smaller cells, presumably TM7x. Inset shows a zoomed-in image of the smaller TM7x (box with dashed line) that seems to be budding. (C) Isolated TM7x using 0.22-micron filter shows cocci TM7x with diameter of ~200 nm. (D) Co-culture grown under anaerobic conditions shows elongated XH001 decorated with many elongated TM7x.

Author Manuscript Author Manuscript Author Manuscript Author Manuscript

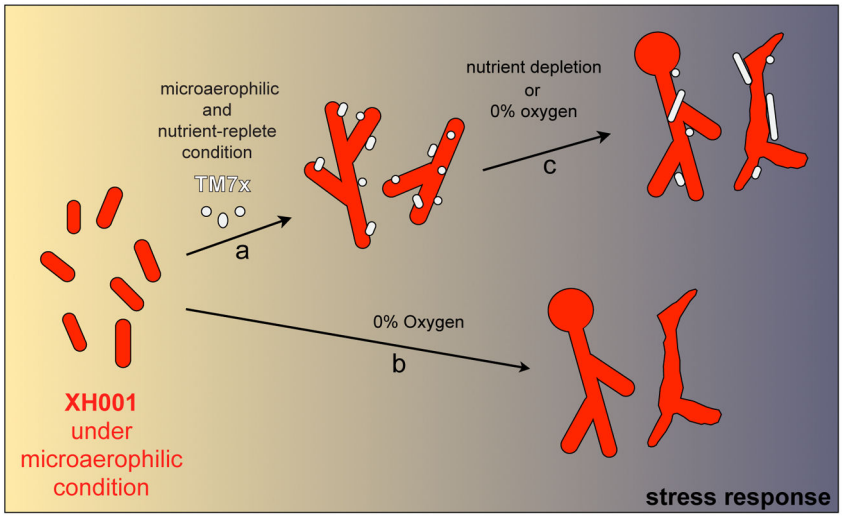


**Figure 8.**

Diagram depicting morphological changes of XH001 and TM7x under different conditions. XH001 and TM7x bacteria are shown in red and gray respectively. Arrows represent the changes in condition of the culture environment: (a) attachment of TM7x to XH001 under microaerophilic nutrient-replete environment, (b) incubation of XH001 alone under oxygen deplete environment, and (c) co-culture under nutrient or oxygen deplete condition. Increasing dark color in the background represents increase in stress response genes.